Dynamical deformation in heavy ion collisions and formation of superheavy nuclei

Minghui Huang,[1] Zhiyuan Zhang,[1,2] Zaiguo Gan,[1] Xiaohong Zhou,[1] Junqing Li,[1,3] and W. Scheid[4]
[1]*Institute of Modern Physics, Chinese Academy of Sciences, Lanzhou 730000, China*
[2]*Graduate University of Chinese Academy of Sciences, Beijing 100049, China*
[3]*School of Nuclear Science and Technology, Lanzhou University, Lanzhou 730000, China*
[4]*Institut für Theoretische Physik, Justus-Liebig-Universität, D-35392 Giessen, Germany*
(Received 17 August 2011; revised manuscript received 21 November 2011; published 28 December 2011)

To develop a dinuclear system conception, dynamical deformation and nucleon transfer in the heavy ion fusion reaction process are viewed simultaneously as a diffusion process and are treated by solving a set of master equations with the variables of the quadrupole deformation of each nucleus and the mass asymmetry variable in the potential energy surface (PES) of the system. The PES is determined by these three variables (two deformation coordinates and the mass asymmetry coordinate) and further governs the variation of the three variables by the master equations. The nucleon transfer and dynamical deformations of nuclei are correlated in the reactions. So the energy surface of the system for nucleon transfer is dependent on deformations and, thus, is time dependent. The calculated results for the quasifission mass yields and the excitation function of the evaporation residue cross sections to form elements 114 and 116 are shown to be agreeable with the measured data.

DOI: 10.1103/PhysRevC.84.064619 PACS number(s): 25.70.Jj, 24.10.−i, 25.60.Pj, 27.90.+b

I. INTRODUCTION

Producing superheavy elements (SHEs) is one of the major aims of modern nuclear heavy ion physics. Searching for the superheavy nuclear island of stability which is predicted theoretically has received much experimental attention with fusion-evaporation reactions [1–9]. However, up to now this island of stability has not been localized in experiments, and further synthesis becomes more and more difficult. A better understanding is needed. In the dinuclear system (DNS) conception the formation of superheavy nuclei (SHN) is discussed as a competition between quasifission (QF) and complete fusion, and the cross sections are calculated including nuclear structure effects. This model not only reproduces the experimental data quite well but also predicts the optimal projectile-target combinations as well as the optimal bombarding energies to form certain SHEs [10–16].

In the DNS conception it is assumed that each of the two touching nuclei always keeps its own identity with its ground-state deformation [10]. However, in the touching configuration, there are nuclear and Coulomb interactions between the nuclei. Nuclei get deformed gradually due to the strong nuclear and Coulomb interactions. This deformation is not negligible and will influence the further evolution of the system, so that the DNS conception has to be improved. However, this dynamical deformation is difficult to describe, and no theory has succeeded in describing it so far, since thorough coupling between the collective and the intrinsic variables is impossible to achieve for heavy ion reactions presently. We take quadrupole deformations of nuclei in the DNS as dynamical variables in addition to the mass asymmetry variable and construct a new three-variable master equation (ME) so that the deformations as well as the nucleon transfer are viewed as a diffusion process consistently governed by MEs in the potential energy surface (PES) of the system. The PES is determined by these three variables. It also governs the variation of the three variables via the MEs. The nucleon transfer and the dynamical deformations of the nuclei are correlated in the reactions. So the PES of the system depends on deformations and is time dependent. The coupling between the deformations, which are the collective variables, and the intrinsic properties of the fragments, such as the shell, pairing, isospin symmetry, and excitation, are not treated explicitly, however, they are correlated via the masses of the fragments as a whole in the PES. On this basis, the competition between fusion leading to SHN and QF is studied, which sheds some interesting light on the reaction mechanism.

The paper is organized as follows. First, we introduce the formalism of our new MEs in Sec. II, and we discuss the trend of the evolution of deformations to equilibrium in Sec. III. The time-relevant potential surface is described in Sec. IV. The calculated mass yields and fusion probabilities are given in Sec. V. In Sec. VI we present our summary.

II. DESCRIPTIONS OF THE MODEL

A. The model

The presently developed DNS starts from a molecular configuration of two touching nuclei. The nuclei gradually get deformed due to the strong nuclear and Coulomb interactions between them. Here only the axially symmetric quadrupole deformations of the nuclei are considered, and we always take the tip-to-tip orientation. Such a system also evolves along two main degrees of freedom: the transfer of nucleons in the mass asymmetry coordinate $\eta = (A_1 - A_2)/(A_1 + A_2)$ between the nuclei in the excited system, leading to compound nuclear formation; and the variation of the internuclear distance r of the nuclei in the interaction potential leading to QF. The evolution of the system is described by the following

ME:

$$\begin{aligned}\frac{dP(A_1,\beta_1,\beta_2,t)}{dt} &= \sum_{A_1'} W_{A_1,\beta_1,\beta_2;A_1',\beta_1,\beta_2}(t)\big[d_{A_1,\beta_1,\beta_2}P(A_1',\beta_1,\beta_2,t) \\ &\quad - d_{A_1',\beta_1,\beta_2}P(A_1,\beta_1,\beta_2,t)\big] \\ &\quad + \int_{\beta_{10}}^{\infty}\int_{\beta_{20}}^{\infty} W_{A_1,\beta_1,\beta_2;A_1,\beta_1',\beta_2'}(t)\big[d_{A_1,\beta_1,\beta_2}P(A_1,\beta_1',\beta_2',t) \\ &\quad - d_{A_1,\beta_1',\beta_2'}P(A_1,\beta_1,\beta_2,t)\big]\rho(\beta_1')\rho(\beta_2')d\beta_1'd\beta_2' \\ &\quad - \Lambda^{qf}_{A_1,\beta_1,\beta_2}(\Theta(t))P(A_1,\beta_1,\beta_2,t), \end{aligned} \tag{1}$$

where $P(A_1,\beta_1,\beta_2,t)$ denotes the probability distribution function to find fragment 1 with A_1 nucleons, the quadrupole deformations of fragments being β_1 and β_2, with the corresponding local excitation energy $E_{A_1,\beta_1,\beta_2}(J)$ at time t and with the incident angular momentum J. β_1 and β_2 are taken as two discrete variables, corresponding to the projectile-like and target-like fragments, respectively. They are taken as continuous variables in the second line of Eq. (1), however, $\rho(\beta_i')=\frac{1}{h_i}$ is the density of the discrete dots with the step length h_i $(i=1,2)$. The local excitation energy is determined by the dissipated energy from the relative motion and the PES of the corresponding DNS [this is shown in Eqs. (7) and (8)]. The dissipation energy is described by the parametrization method of the classical deflection function [17,18]. $W_{A_1,\beta_1,\beta_2;A_1',\beta_1,\beta_2}(t)=W_{A_1',\beta_1,\beta_2;A_1,\beta_1,\beta_2}(t)$ [also $W_{A_1,\beta_1,\beta_2;A_1,\beta_1',\beta_2}(t)=W_{A_1,\beta_1',\beta_2;A_1,\beta_1,\beta_2}(t)$ and $W_{A_1,\beta_1,\beta_2;A_1,\beta_1,\beta_2'}(t)=W_{A_1,\beta_1,\beta_2';A_1,\beta_1,\beta_2}(t)$] is the mean transition probability from channel (A_1,β_1,β_2) to channel (A_1',β_1,β_2) [also from (A_1,β_1,β_2) to (A_1,β_1',β_2) and to (A_1,β_1,β_2')]. Simultaneous variable transitions are not considered. The details of the calculation of the transition probability are presented in the Appendix. d_{A_1,β_1,β_2} denotes the microscopic dimension corresponding to the macroscopic state (A_1,β_1,β_2). The sum is taken over all possible mass numbers that a fragment A_1' may take, but only one-nucleon transfer is considered. To solve the three-variable partial differential equations numerically, a three-step difference scheme is adopted. The lower limit of deformations is $\beta_{10,20}=0$ if the initial deformations $\beta_{P,T}>0$; otherwise, $\beta_{10,20}=-0.6$.

In principle, the relative internuclear distance and orientation could also be taken as dynamical variables in the ME [21], but presently the computation time is much too long. So a tip-to-tip relative orientation is assumed and the nuclei stay in the bottom of the pocket to keep the lowest potential, which determines the relative distance of nuclei. We keep the conditions for this relative orientation and the relative distance of nuclei throughout the current calculations. In this DNS, the fusion process to form a compound nucleus is competing with QF, which can be described by incorporating Kramer's formula (KF) into the ME, Eq. (1) [22–24]. It is proved that KF works well in the mass asymmetry region where the QF barriers are high [25]. The QF rate $\Lambda^{\rm qf}_{A_1,\beta_1,\beta_2}[\Theta(t)]$ is estimated with KF [23,26]:

$$\Lambda^{\rm qf}_{A_1,\beta_1,\beta_2}(\Theta(t)) = \frac{\omega}{2\pi\omega^{B_{\rm qf}}}\left(\sqrt{\left(\frac{\Gamma}{2\hbar}\right)^2+(\omega^{B_{\rm qf}})^2}-\frac{\Gamma}{2\hbar}\right) \times \exp\left(-\frac{B_{\rm qf}(A_1,\beta_1,\beta_2)}{\Theta(t)}\right). \tag{2}$$

Here the QF barrier $B_{\rm qf}$ is the depth of the pocket of the interaction potential. The local temperature is given by the Fermi-gas expression $\Theta=\sqrt{\varepsilon^\star/a}$, with the level density parameter $a=A/12$ MeV^{-1} and the local excitation energy $\varepsilon^\star$. The frequency $\omega^{B_{\rm qf}}$ is the frequency of the inverted harmonic oscillator approximating the interaction potential of two nuclei along the internuclear distance around the top of the QF barrier, and ω is the frequency of the harmonic oscillator approximating the potential along the internuclear distance around the bottom of the pocket. The quantity Γ denotes the double-average width of the contributing single-particle states. Here constant values $\Gamma=2.8$ MeV, $\hbar\omega^{B_{\rm qf}}=2.0$ MeV, and $\hbar\omega=3.0$ MeV were used. The QF yield is finally obtained with

$$Y^{\rm qf}_{A_1}(J) = \int_{t=0}^{\tau_{\rm int}}\int_{\beta_{10}}^{\infty}\int_{\beta_{20}}^{\infty}\Lambda^{\rm qf}_{A_1,\beta_1,\beta_2}(\Theta(t)) \times P(A_1,\beta_1,\beta_2,t)\rho(\beta_1)\rho(\beta_2)d\beta_1d\beta_2dt. \tag{3}$$

The fusion probability is

$$P_{\rm CN}(J) = \sum_{A_1=1}^{A_{\rm BG}}\int_{\beta_{10}}^{\infty}\int_{\beta_{20}}^{\infty}P(A_1,\beta_1,\beta_2,\tau_{\rm int})\rho(\beta_1)\rho(\beta_2)d\beta_1d\beta_2. \tag{4}$$

The initial condition is $P(A_P,\beta_P,\beta_T,t=0)=1$, where A_P is the mass number of the projectile. The interaction time $\tau_{\rm int}$ in the dissipative process of two colliding nuclei is dependent on the incident energy $E_{\rm c.m.}$ and the incident angular momentum J, which is determined by using the deflection function method [25], and $\tau_{\rm int}$ has the value of the magnitude from a few to several hundred 10^{-22} s.

B. Potential energy of the DNS

In the relaxation process of relative motion, the DNS will be excited by the dissipation of the relative kinetic energy. The local excitation energy is determined by this transferred excitation energy of the composite system and the PES of the DNS. The PES is given by

$$\begin{aligned}U(A_1,A_2,R,\beta_1,\beta_2,J) &= E(A_1,\beta_1)+E(A_2,\beta_2)-\big[E(A_{\rm CN},\beta_{\rm CN})+V^{\rm CN}_{\rm rot}(J)\big] \\ &\quad + V_{\rm CN}(A_1,A_2,R,\beta_1,\beta_2,J),\end{aligned} \tag{5}$$

where $A_{\rm CN}=A_1+A_2$ is the mass number of the compound nucleus and β_i represent the quadrupole deformation of the two fragments. Nucleon transfer begins from the injection point channel by losing or gaining one nucleon, and whether it should be a neutron or a proton depends on which of them would make the potential energy lower. R is the distance

between nuclei at which the interaction potential between the two nuclei $V_{\rm CN}(A_1, A_2, R, \beta_1, \beta_2, J)$ has the minimum value. $E(A_i, \beta_i)$ $(i = 1, 2)$ and $E(A_{\rm CN}, \beta_{\rm CN})$ are the total energies of the ith nucleus and the compound nucleus, respectively, in which the shell and the pairing corrections are included. They can be calculated as a sum of the liquid drop energy and the Strutinsky shell correction. We use the formula and parameters from Ref. [27]:

$$E(A_i, \beta_{i2}) = E_{\rm LD}(A_i) \prod_{k=2 \text{ and } 4} \left(1 + b_{ik}\beta_{ik}^2\right) + c_1 E_{\rm shell}(A_i, \beta_{ik}), \quad (6)$$

where only axially deformed cases β_{i2} and β_{i4} are considered and, in this context, the notation $\beta_i \equiv \beta_{i2}$. The energy of a nucleus with respect to the axial deformations is calculated with a Skyrme energy-density functional together with the extended Thomas-Fermi approximation, which gives the minimum total energies of the ith nucleus with the optimal values β_{i2}, β_{i4}(the β_{i4} is not of further using here). The binding energy and the deformation of the ground state (DGS) obtained with this formula are very close to the results in Möller's table [28].

The $V_{\rm rot}^{\rm CN}$ is the rotation energy of the compound nucleus. The interaction potential between the two nuclei $V_{\rm CN}(A_1, A_2, R, \beta_1, \beta_2, J)$ includes the nuclear, Coulomb interaction, and centrifugal parts; the details are given in Ref. [29].

In the relaxation process of the relative motion, the DNS will be excited by the dissipation of the relative kinetic energy. The excited system opens a valence space $\Delta\varepsilon_K$ in each fragment K $(K = 1, 2)$, which has a symmetrical distribution around the Fermi surface. Only the particles in the states within this valence space are actively involved in the excitation and transfer.

$$\Delta\varepsilon_K = \sqrt{\frac{4\varepsilon_K^*}{g_K}}, \quad \varepsilon_K^* = \varepsilon^* \frac{A_K}{A}, \quad g_K = \frac{A_K}{12}, \quad (7)$$

where ε^* is the local excitation energy of the DNS, which provides the excitation energy for the mean transition probability. There are $N_K = g_K \Delta\varepsilon_K$ valence states and $m_K = N_K/2$ valence nucleons in the valence space $\Delta\varepsilon_K$, which gives the dimension $d(m_1, m_2) = \binom{N_1}{m_1}\binom{N_2}{m_2}$. The local excitation energy is defined as

$$\varepsilon^* = E_x - U(A_1, A_2, R, \beta_1, \beta_2, J). \quad (8)$$

The excitation energy E_x of the composite system is converted from the relative kinetic energy loss, which is related to the Coulomb barrier [29] and is determined for each initial relative angular momentum J by the parametrization method of the classical deflection function [17,30]. So E_x is coupled with the relative angular momentum.

III. EVOLUTION OF THE DEFORMATIONS

In Fig. 1 we show the interaction PES as a function of the quadrupole deformations for the reaction ^{48}Ca + ^{244}Pu at entrance channel $A_1 = 48$. The relative distance between nuclei is taken to be the value which gives the the minimum

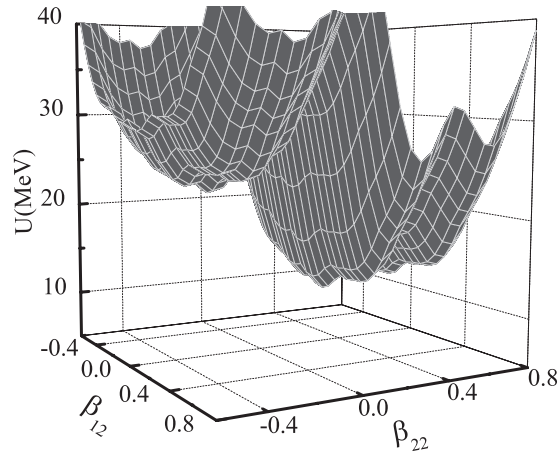

FIG. 1. PES for the reaction ^{48}Ca + ^{244}Pu as a function of quadrupole deformations in the entrance channel $(A_1 = 48)$.

PES, and the same for later cases. We find that the lowest potential region sits in the range $\beta_{i2} > 0$. The deformations of the entrance channel are $\beta_{12} = 0.0$ and $\beta_{22} = 0.215$. So the nuclear shapes trend toward keeping prolate ellipsoidal shapes in the fusion process. This condition also exists at other mass asymmetries.

For a different mass asymmetry channel, the shape of the PES is quite different. The part of the PES in the positive deformation region of the reaction ^{48}Ca + ^{244}Pu for $A_1 = 48$ and $A_1 = 86$ is shown in Figs. 2(a) and 2(b), respectively. Point I in Fig. 2(a) is the incident channel. Values in parentheses are the deformations of projectile-like and target-like nuclei, respectively.

For $A_1 = 48$ the lowest minimum is at position A in a region with a small deformation ($\beta_{12} = 0.1$, $\beta_{22} = 0.25$) near the incident point. The second minimum is at point B, where the heavy fragment has a large deformation ($\beta_{12} = 0.1$, $\beta_{22} = 0.6$). While for $A_1 = 86$ the system is more symmetric, heavier nuclei can have a larger deformation due to the larger Coulomb repulsion. The two minimum potential energies are located at $\beta_{12} = 0.2$, $\beta_{22} = 0.05$ (point C) and $\beta_{12} = 0.2$, $\beta_{22} = 0.45$ (point D).

In order to present an overview about deformation and how it evolves with time during the dynamical reaction process, we should check how the distribution function is distributed with respect to the corresponding deformations. We show the time evolution of the probability function $P(A_1, \beta_1, \beta_2, t)$ as a function of deformations in Fig. 3 for the entrance channel $A_1 = 48$. From the beginning of the reaction up to $t = 2 \times 10^{-22}$ s, the probability function is distributed around the injection point (point A), with $\beta_{12} = 0.0$ and $\beta_{22} = 0.215$. With increasing time it diffuses, to be distributed over a wider area with wider nuclear deformations. At $t = 50 \times 10^{-22}$ s, an appreciable probability is accumulated at the second potential minimum (point B). For the configuration $A_1 = 86$ (see Fig. 4) at $t = 10 \times 10^{-22}$ s, the maximum probability of the distribution function is already located at the minimum position of the potential [point D in Fig. 2(b)]. With increasing time, the probability is continuously accumulated

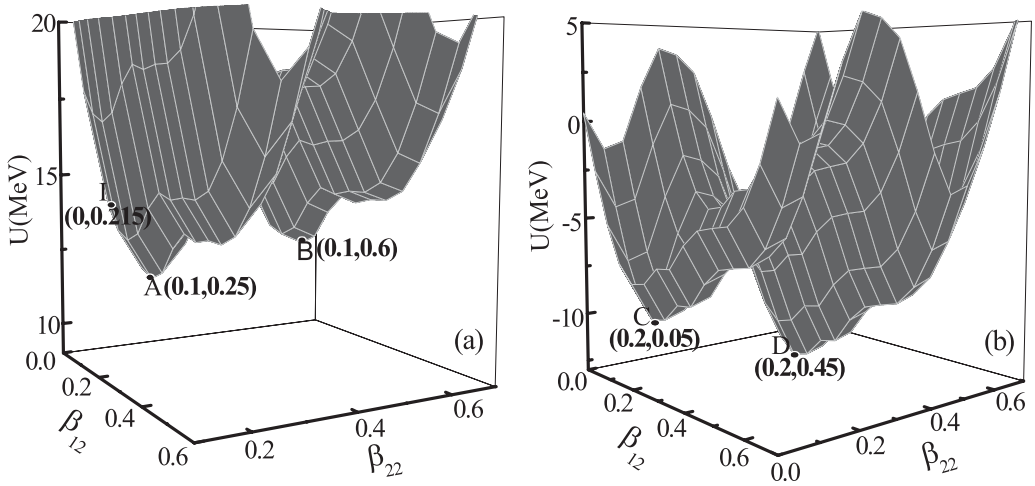

FIG. 2. Part of the PES in the positive deformation region of the reaction ^{48}Ca + ^{244}Pu at $A_1 = 48$ (a) and $A_1 = 86$ (b). Point I is the incident channel. Values in parentheses are the deformations of projectile-like and target-like nuclei, respectively.

at point D and diffuses widely to other deformations. At $t = 100 \times 10^{-22}$ s, besides at point D, there is also a small peak at the second minimum of the potential [point C in Fig. 2(b)].

The variation ratio of the distribution probability function at points A and B in Fig. 2, i.e., (P(B)/P(A)), as well as that at points C and D, (P(C)/P(D)), is shown in Fig. 5 as a function of the interaction time (solid line and dotted line, respectively).

For each value of η, the distribution probability finally reaches equilibrium. For the entrance channel $A_1 = 48$, the distribution probability reaches equilibrium with respect to deformations at about $t = 60 \times 10^{-22}$ s; and for $A_1 = 86$, at about $t = 100 \times 10^{-22}$ s. The longer equilibrium time for the latter case is due to the sequential nucleon transition to reach the considered channel, i.e., a 38-nucleon transfer is needed to reach the channel first. For the channel $A_1 = 86$, until $t = 50 \times 10^{-22}$ s, the distribution probability P(D) increases to 2.2×10^{-3}, and only then do other deformations appear. However, nucleon transfer is not the only factor that influences the shape relaxation. Naturally, the PES plays a very important

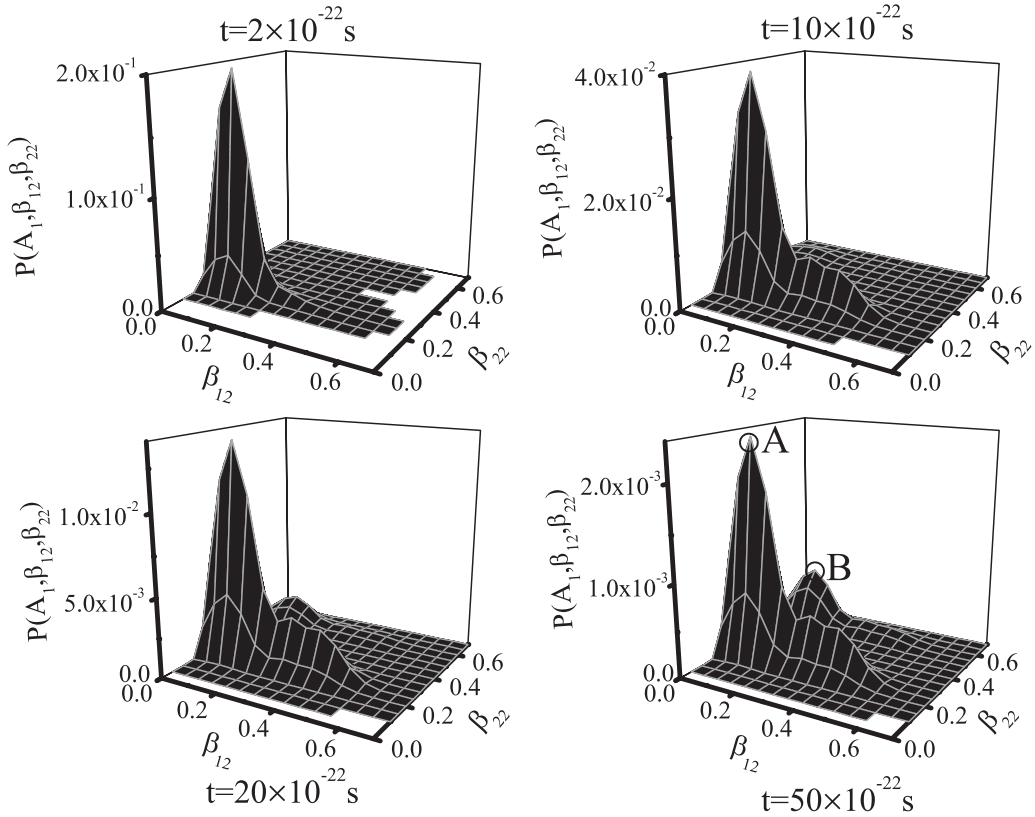

FIG. 3. Probability distribution as a function of deformations of the reaction ^{48}Ca + ^{244}Pu at different interaction times for $A_1 = 48$.

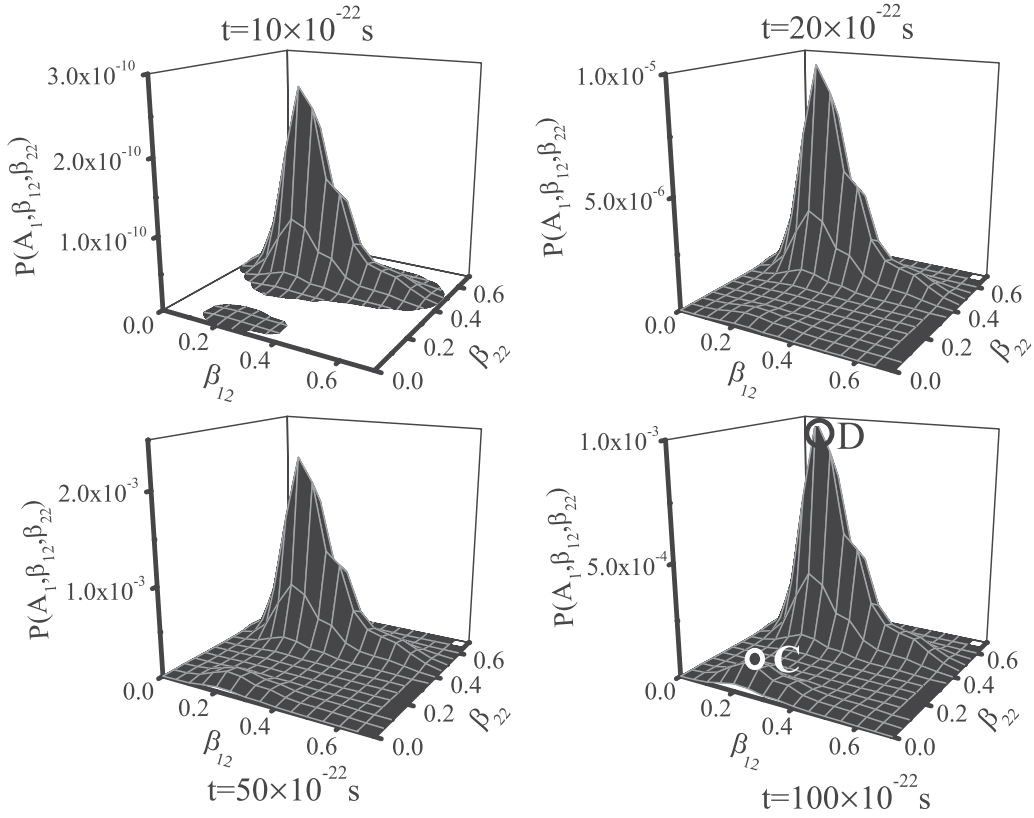

FIG. 4. Probability distribution as a function of deformations of the reaction ^{48}Ca + ^{244}Pu at different interaction times for $A_1 = 86$.

role. An example is the channel $A_1 = 58$. Its PES is shown in Fig. 6(a), with two minima in the PES, indicated by E and F. The ratio of the probability distribution between E and F is shown as a function of the reaction time in Fig. 6(b). The ratio reaches its equilibrium around $t = 20 \times 10^{-22}$ s, which is shorter than that for the entrance channel, although a nucleon transfer is not needed there. The reason can be drawn from Fig. 7, where the probability distributions for $A_1 = 58$ as a function of the deformations for the reaction ^{48}Ca + ^{244}Pu at different interaction times are shown. We find that the probability is first distributed at point E, then gradually at other places, and finally, two peaks are formed. The peak at F is higher than that at E. From Fig. 6(a) it can be seen that from point E to point F, there is a barrier $B_{\rm EF} = 0.78$ MeV. In the entrance channel $A_1 = 48$ the barrier from A to B is 4.97 MeV, and in the channel $A_1 = 86$ the barrier from D to C is 8.54 MeV. The barrier in Fig. 6(a) is much lower than those in the channels with $A_1 = 48$ and 86. This is the very reason that the equilibrium time for the channel $A_1 = 58$ is shorter, although 10 nucleons must first be transferred to reach this channel.

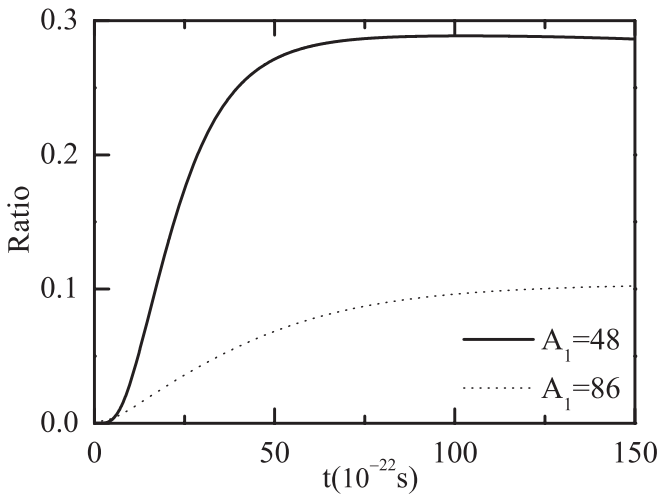

FIG. 5. The solid line denotes the variation of the probability ratio (P(B)/P(A)) with the interaction time of peaks B and A in Fig. 3; the dotted line denotes the ratio (P(C)/P(D)) of peaks C and D in Fig. 4.

IV. THE TIME-RELEVANT POTENTIAL ENERGY SURFACE

The variation of the distribution probability $P(A_1, \beta_1, \beta_2, t)$ at time t is the distribution probability which is transferred from the neighboring configurations to the considered configuration minus the distribution probability transferred from the considered configuration to the neighboring configurations. Therefore, the rate depends on the transition probability, which is determined by the PES, and on the magnitude of the corresponding distribution probability. So the transition probability and the magnitude of the distribution probability

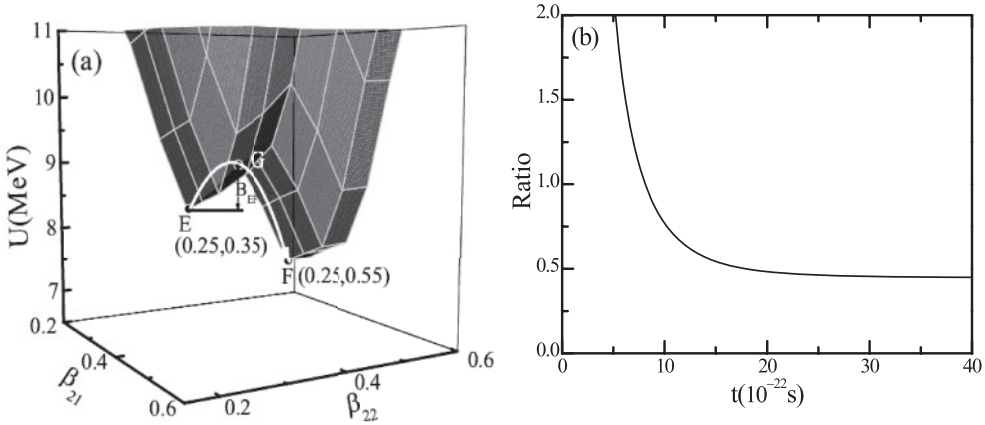

FIG. 6. (a) Part of the PES in the positive deformation region of the reaction ^{48}Ca + ^{244}Pu at $A_1 = 58$ with the nuclei at the bottom of the potential pocket. (b) Variation of the probability ratio (P(E)/P(F)) with the interaction time of points E and F in (a).

are both important. For each mass asymmetry A_1, the distribution probability is distributed corresponding to the nuclear deformations, which determine the corresponding PES. The configuration which has the maximum distribution probability has the greatest possibility of transferring a nucleon to its neighboring configuration in the mass asymmetry variable. The PES with the maximum distribution probability for different evolution times is shown in Fig. 8 for the reaction ^{48}Ca + ^{244}Pu as a function of A_1. The upper line is the PES with ground-state deformations (at $t = 0 \times 10^{-22}$ s). With increasing time, as indicated in the figure, the PES gets lower, but the rate of decrease gets smaller and smaller. And the more the mass asymmetry decreases, the lowering of the PES is due to the larger Coulomb interaction between the nuclei, which lead to nuclear deformations. This argues in favor of the distribution probability's being distributed in the symmetric region. The QF barrier is usually lower for the symmetric DNS. So the QF of the system is affected. However, the PES in the very mass asymmetric region is not distinctly affected, which gives less support for fusion.

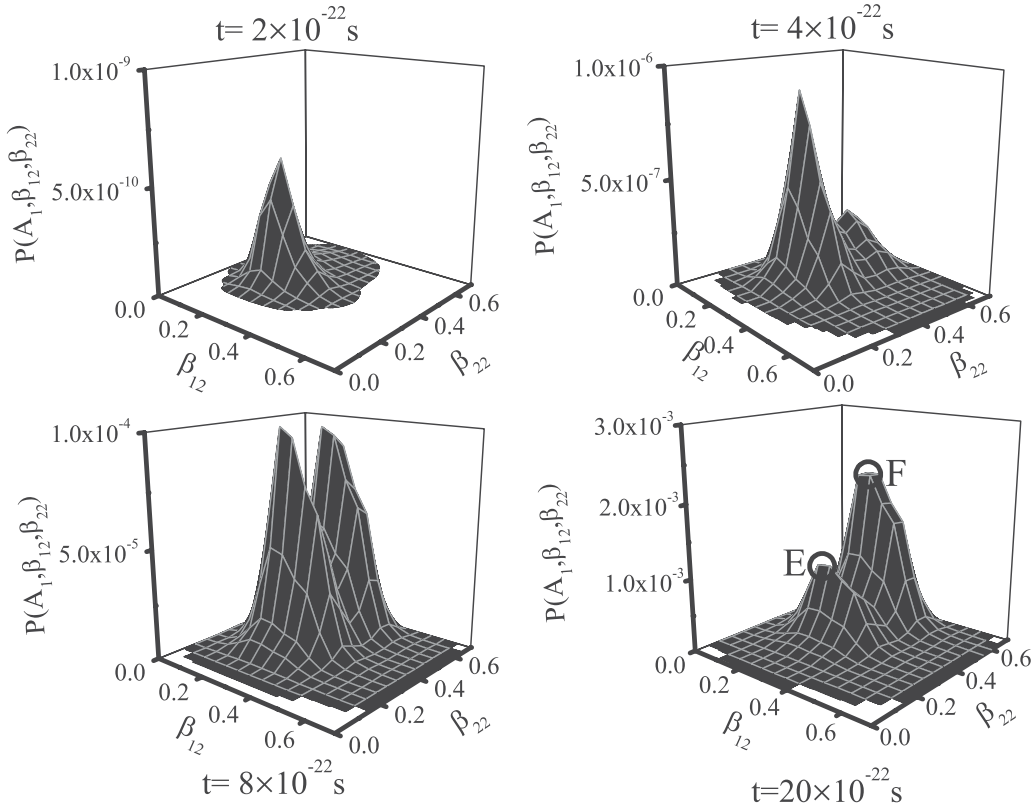

FIG. 7. Probability distribution as a function of deformations of the reaction ^{48}Ca + ^{244}Pu at different interaction times for $A_1 = 58$.

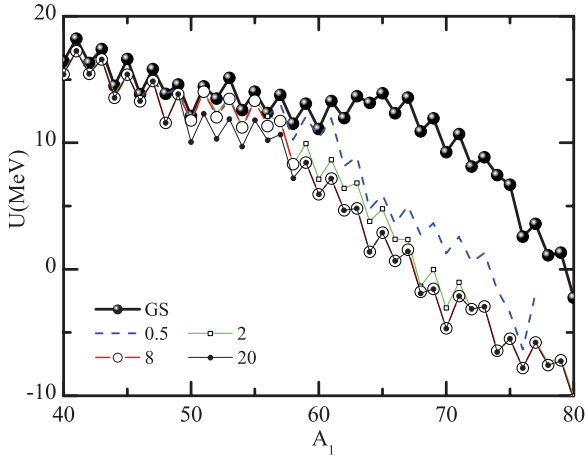

FIG. 8. (Color online) The PES with the maximum distribution probability for different evolution times for the reaction ^{48}Ca + ^{244}Pu. GS, 0.5, 2, 8, and 20 indicate the interaction times $t = 0$, 0.5, 2, 8, and 20 $\times$ 10^{-22} s, respectively.

In order to determine the time evolution of the deformations, we define the mean value of a deformation as

$$\overline{\beta_{i2}}(A_1, t) = \frac{1}{C}\int_{\beta_{10}}^{\infty}\int_{\beta_{20}}^{\infty} P(A_1, \beta_{12}, \beta_{22}, t)\beta_{i2}d\beta_{12}d\beta_{22},$$
$$C = \int_{\beta_{10}}^{\infty}\int_{\beta_{20}}^{\infty} P(A_1, \beta_{12}, \beta_{22}, t)d\beta_{12}d\beta_{22}, \quad (9)$$

where β_{10} and β_{10} are defined after Eq. (1). For the same reaction channel and for each mass asymmetry, the mean value of the quadrupole deformation parameters of fragments A_1 and A_2 at different reaction times are presented in Fig. 9, respectively. Note that the abscissa is the mass number of fragment 1. With increasing time, the mean deformation generally increases. The increasing magnitude decreases with increasing time. In the symmetric region, with increasing time, the deformation gets quite different from that in the ground state, while in the asymmetric region there is not much difference.

V. THE QF YIELD AND FUSION PROBABILITY

In the reaction process, the variation along the relative distance between the nuclei leads to QF is described by Eq. (2). Actually in heavy ion induced reactions, some experiments show that the deep inelastic and QF processes are the dominant reaction channels [31,32]. The QF mass yields often indicate some details of reaction dynamics.

For the entrance channel of ^{48}Ca + ^{244}Pu, the QF barrier $B_{\rm qf}$ is shown in Fig. 10(a) as a function of the relative distance of the nuclei, and in Fig. 10(b) the barriers are shown as function of the deformations of fragments. We see smaller QF barriers at larger deformations, which are favorable for QF.

The QF mass yields of the reaction ^{48}Ca + ^{244}Pu with $E^* = 33$ MeV are shown by solid lines in Figs. 11(c) and 11(d), obtained by using the one-variable ME [15,16] with the deformation at ground state (DGS) and by using the current

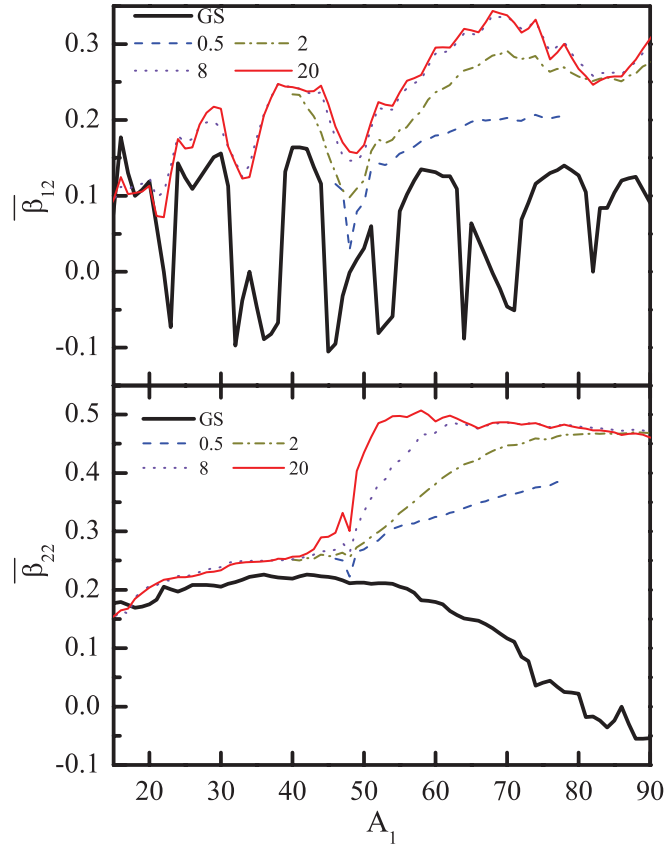

FIG. 9. (Color online) Mean values of the deformations of fragments A_1 and A_2 at different reaction times for the reaction ^{48}Ca + ^{244}Pu. GS, 0.5, 2, 8, and 20 indicate the times $t = 0$, 0.5, 2, 8, and 20 $\times$ 10^{-22} s, respectively.

ME with deformations evolving with time (DET), respectively. In Fig. 11(c), there are two high peaks at mass numbers 61 and 106, corresponding to two minima of the PES in Fig. 11(a). This is not consistent with the experimental data. Furthermore, the QF yield falls down about three orders of magnitude at mass number 113 because a high peak appears in the PES in Fig. 11(a) for this mass asymmetry. The reason is that the ground-state deformation of the light nucleus abruptly changes from 0.328 (at $A_1 = 112$) to -0.258 (at $A_1 = 113$) [25]. By considering the deformations of the nuclei as dynamical variables, the variation of the deformations is governed by Eq. (1) in the PES of the system, and the PES is dependent on the deformations. Thus we get reasonable deformations. For the case where the deformations reached equilibrium, the PES and QF yields obtained with the current method are shown in Figs. 11(b) and 11(d), respectively. In Fig. 11(d) it is shown that the highest peak is at mass number 86, with the heavy fragment close to ^{208}Pb, reflecting the shell effects. It corresponds to a minimum of the PES in Fig. 11(b) and agrees rather well with the experimental data, although the peak is a little lower than the experimental one. However, in the range of the rectangle, the mass intervals of the experimental points are about 2, and those of our calculated ones are equal to 1. On the other hand, the error bars of the data are greater than 2 [3,32]. One should note that the total yields of the measured data and

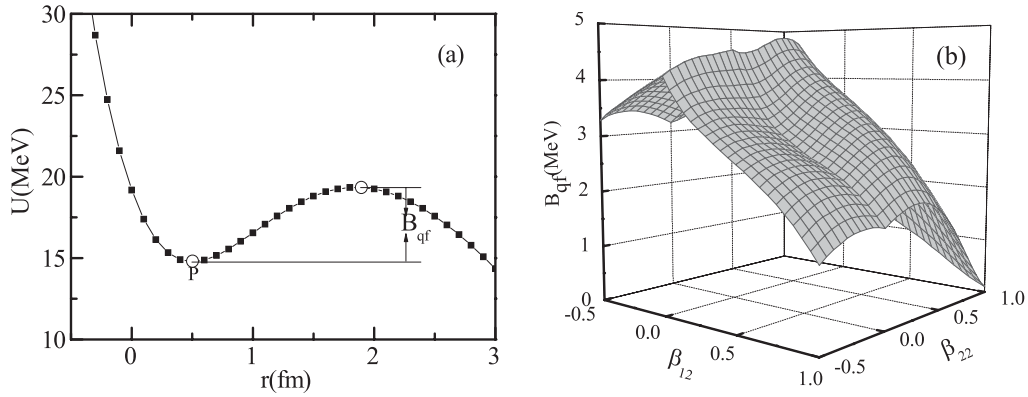

FIG. 10. (a) Interaction potential between colliding nuclei in the entrance channel along the internuclear distance for the reaction ^{48}Ca + ^{244}Pu. (b) QF barrier related to quadrupole deformations with the entrance channel A_1.

of our calculation in the rectangular area (mass numbers 67 to 104) are 0.612 and 0.656, respectively. The two values are very close.

We also calculated the QF yields of the reactions ^{48}Ca + ^{248}Cm and ^{48}Ca + ^{238}U with $E^* = 33$ MeV, which are displayed by filled squares in Figs. 12(a) and 12(b), respectively. The highest peaks of the two distributions are at mass numbers $A_1 = 90$ and $A_1 = 84$, respectively, and fit the data quite well. It is worth mentioning that the authors of Ref. [23] found a sharp QF yield peak at $A_1 = 43$ for each of the above-mentioned three reactions. This phenomenon does not exist in our results. The dynamical treatment of the system populates the considered dynamical variables correctly. The treatment of the dynamical deformations of the nuclei of the DNS can describe the distribution of the QF yields better than the treatment considering only the deformations of their ground states. This demonstrates the necessity of considering the time-dependent deformation.

Figure 8 indicates that the more the mass asymmetry decreases, the more the PES decreases. In the region of large mass asymmetry, the PES does not change much. The consequence is that this variation of the potential influences QF greatly, but not fusion.

The fusion probability for collisions of ^{48}Ca + ^{244}Pu with $J = 0$ is shown in Fig. 13(c) as a function of the excitation energy. The filled squares, $P_{\rm CN}^{\rm DET}$, are from the current calculation (called the DET case), and the results calculated with $P_{\rm CN}^{\rm DGS}$ using the ground-state deformations (called the DGS case, obtained with a one-variable ME) are indicated by open circles. It is found that in the low-energy region, $E^* < 40$ MeV, the difference in the two results is not very large. At $E^* > 37$ MeV, $P_{\rm CN}^{\rm DET} < P_{\rm CN}^{\rm DGS}$, and at lower excitation energies, $P_{\rm CN}^{\rm DET} > P_{\rm CN}^{\rm DGS}$ [see Fig. 13(c)]. The PESs for the two cases are shown in Fig. 13(a). The difference between the PESs in the very asymmetric region is small. However, a small variation in the shape of the PES changes the inner fusion barrier from

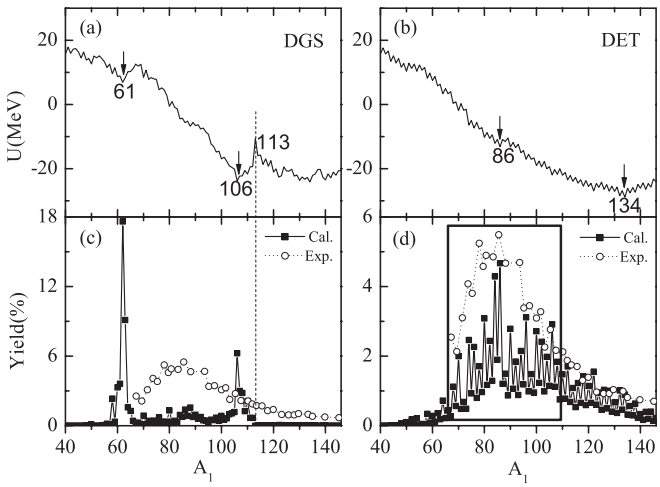

FIG. 11. (a, c) PES and QF yields for ^{48}Ca + ^{244}Pu at $E^* = 33$ MeV along the mass asymmetry degrees of freedom using the DGS obtained from Möller's table [28]. (b) PES with equilibrium deformations (at a large interaction time when the deformations in each mass asymmetry channel have already reached equilibrium). (d) QF yield with the method of DET. In (c) and (d), experimental data are denoted by circles.

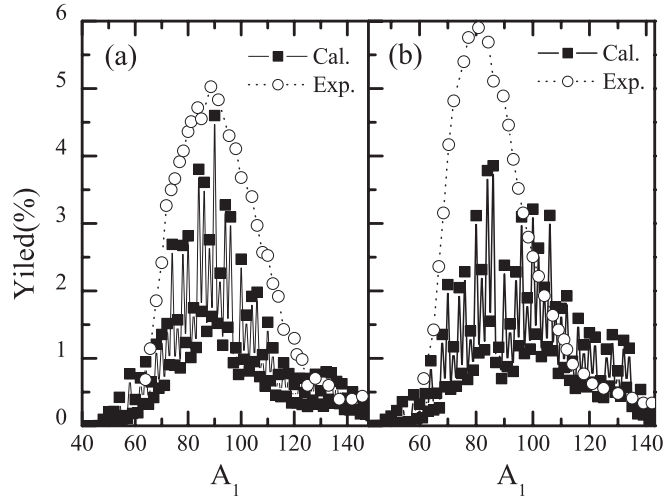

FIG. 12. Mass yields of the reactions ^{48}Ca + ^{248}Cm (a) and ^{48}Ca + ^{238}U (b) at $E^* = 33$ MeV compared with the experimental data.

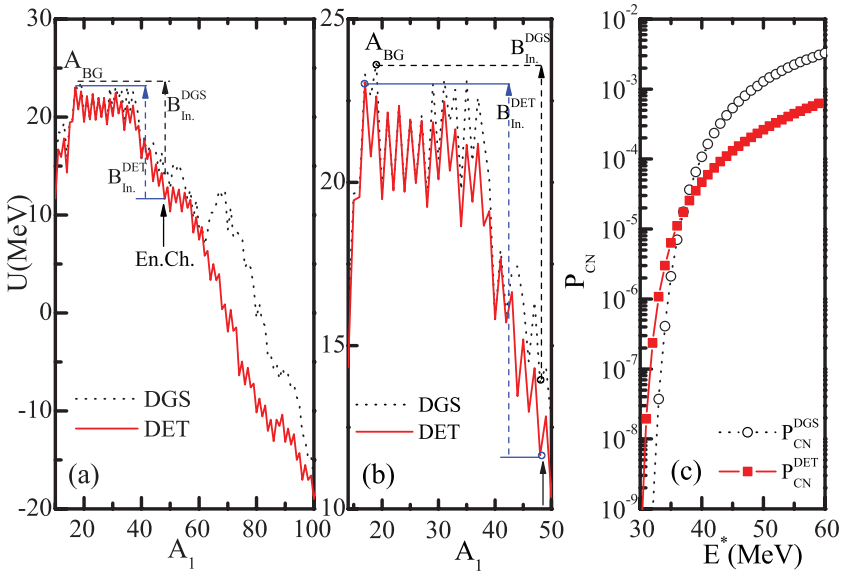

FIG. 13. (Color online) (a) Comparison of the inner fusion barrier using DGS vs DET. One of the arrows indicates the entrance channel. (b) An enlargement of the upper part of (a). (c) Fusion probabilities related to the excitation energy at zero incident angular momentum using DGS vs DET.

$B_{\text{In.}}^{\text{DGS}} = 9.8$ MeV to $B_{\text{In.}}^{\text{DET}} = 11.4$ MeV. Nevertheless, the highest point for the case of DET is lower than that for DGS. So at a low excitation energy the fusion probability for the DET case is higher. With increasing excitation energy, a large proportion of the distribution probability goes down the potential to the mass symmetrical region and to the QF channel. Then the fusion probability becomes lower. A comparison of the excitation function of the evaporation residue cross sections among the results using DGS (dotted lines), DET (solid lines), and available data [33,34] for the reactions ^{48}Ca + ^{244}Pu and ^{48}Ca + ^{248}Cm is shown in Figs. 14(a) and 14(b), respectively. In Fig. 14(a) the maximum values of the two methods for the $2n$, $3n$, and $4n$ channels are similar, because in this energy region, the fusion probability is similar for the two cases. Only the DGS predicts higher optimum excitation energies, except for the $5n$ channel, where the two methods predict the same optimum excitation energy. Since in this higher energy region, at about $E^* > 45$ MeV, the fusion probability for DET is lower than that for DGS, the experimental data for the $5n$ channel [3] are closer to the line calculated with DET. The other experimental data for the $3n$ and $4n$ channels from Dubna [33] and TASCA [34] are distributed among the corresponding lines calculated with the two methods. For the channel ^{48}Ca + ^{248}Cm, the theoretical investigation shows that the results of the two methods show the same behavior with excitation energy.

VI. SUMMARY AND DISCUSSION

This work basically starts with the conception of the DNS . However, the strong nuclear and Coulomb interactions between the nuclei of the DNS make the nuclei become gradually deformed. These deformations will influence the further evolution of the DNS and are not negligible. So the nuclei of the DNS cannot always keep their ground-state deformations. In addition to the mass asymmetry variable, we treat the quadrupole deformations of the nuclei in the DNS as

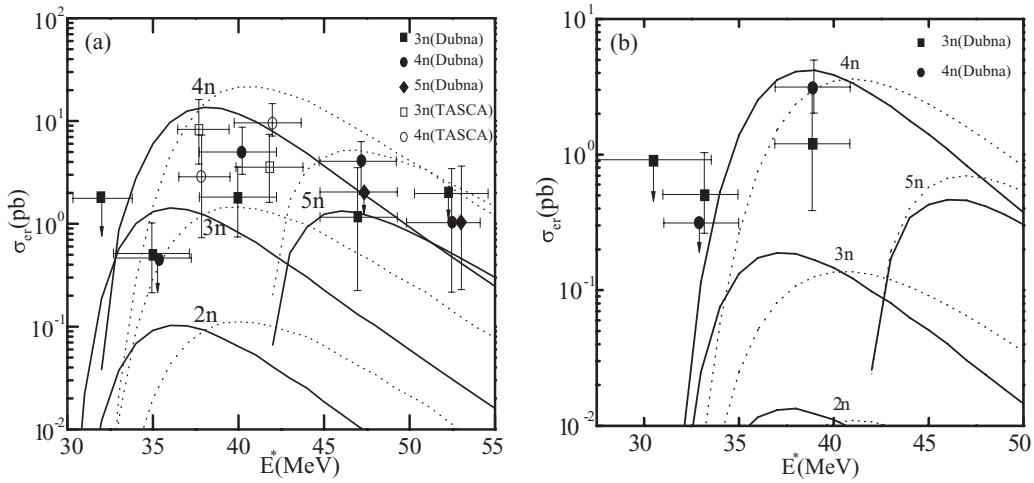

FIG. 14. Comparison of the evaporation residue cross sections among the results using DGS (dotted lines), DET (solid lines), and available data of Dubna [33] and of TASCA [34] for the reactions (a) ^{48}Ca + ^{244}Pu and (b) ^{48}Ca + ^{248}Cm.

dynamical variables and have constructed a new three-variable ME so that the deformations as well as the nucleon transfer are viewed as diffusion processes consistently governed by MEs in the PES. Due to the dynamical treatment the distribution probability of the system is populated reasonably with respect to the variables considered. For each mass asymmetry, the PES is obtained as a function of the fragment deformations. The deformations which give the minimum PES are determined, and the time for the system to reach deformation equilibrium is estimated and found to be different for different mass asymmetries. The PES with the maximum distribution probability at different evolution times reveals the effect of the dynamical deformation: the PES has changed, and therefore, the diffusion dynamics has also changed. The calculated QF yield distribution is greatly improved to fit the data, and the evaporation residue cross sections for ^{48}Ca + ^{244}Pu to produce element 114 and ^{48}Ca + ^{248}Cm to produce element 116 are also reasonably well described. However, we used the approximation of the constant parameters $\Delta_{k,k'}$ and $\gamma_{k,k'}$ in the single-particle interaction matrix element (see the Appendix), independent of the deformations, which is very crude from the physical point of view. We will study this effect in further work.

ACKNOWLEDGMENTS

The work was supported by the National Natural Science Foundation of China (Grant Nos. 10875152, 11175074, 11105035, 10805061, 10825522, 11120101005, and 10975064), the Knowledge Innovation Project of the Chinese Academy of Sciences (Grant No. KJCX2-EW-N01), the Major State Basic Research Development Program (Grant No. 2007CB815000), and the DFG of Germany.

APPENDIX: THE TRANSITION PROBABILITY *W*

The single-particle Hamiltonian to describe the nucleon's motion reads

$$H(t) = H_0(t) + V(t), \tag{A1}$$

$$H_0(t) = \sum_k \sum_{\nu_k} \varepsilon_{\nu_k}(t) a^\dagger_{\nu_k}(t) a_{\nu_k}(t), \tag{A2}$$

$$V(t) = \sum_{k,k'} \sum_{\alpha_k,\beta_{k'}} u_{\alpha_k,\beta_{k'}}(t) a^\dagger_{\alpha_k}(t) a_{\beta_{k'}}(t) = \sum_{k,k'} V_{k,k'}(t), k, k' = 1, 2, \tag{A3}$$

where k, k' ($k, k' = 1, 2$) denote fragment 1 or 2. $\varepsilon_\nu(t)$ and $u_{\nu\mu}(t)$ are the single-particle energy level and interaction matrix element, respectively [14,15,20]. The single-particle states are defined with respect to the centers of the interacting nuclei and are assumed to be orthogonalized in the overlap region. So the annihilation and creation operators are dependent on time. The single-particle matrix elements are parameterized by

$$u_{\alpha_K,\beta_{K'}}(t) = U_{K,K'}(t)\left\{\exp\left[-\frac{1}{2}\left(\frac{\varepsilon_{\alpha_K}(t) - \varepsilon_{\beta_{K'}}(t)}{\Delta_{K,K'}(t)}\right)^2\right] - \delta_{\alpha_K,\beta_{K'}}\right\}, \tag{A4}$$

which contains five fixed independent parameters $U_{11}(t)$ and $U_{22}(t)$ for exciting a nucleon in fragments 1 and 2, respectively, and $U_{12}(t) = U_{21}(t)$ for transferring a nucleon between the fragments, and the corresponding width parameters $\Delta_{11}(t) = \Delta_{22}(t)$ and $\Delta_{12}(t) = \Delta_{21}(t)$. The detailed calculation of these parameters is described in Refs. [37] and [38]. The strength parameters are given by

$$U_{kk'} = \frac{g_1^{\frac{1}{3}} g_2^{\frac{1}{3}}}{g_1^{\frac{1}{3}} + g_2^{\frac{1}{3}}} \frac{1}{g_k^{\frac{1}{3}} g_{k'}^{\frac{1}{3}}} 2\gamma_{kk'}, \tag{A5}$$

with $g_k = A_k/12$, and the reduced strength parameters $\gamma_{11} = \gamma_{22} = \gamma_{12} = \gamma_{21} = \gamma = 3$ [14,19,37,38].

The transition probability from the initial configuration $\xi\{A_1, \beta_1, \beta_2\}$ to the final configuration $\xi\{A_1', \beta_1', \beta_2'\}$ reads

$$W_{\xi,\xi'}(t) = \frac{\tau_{\rm mem}(\xi, \xi\prime)}{\hbar^2 d_\xi d_{\xi'}} \sum_{ii'} |\langle \xi', i'|V|\xi, i\rangle|^2, \tag{A6}$$

where i denotes all remaining quantum numbers. The memory time is

$$\tau_{\rm mem}(\xi, \xi') = (2\pi)^{1/2}\hbar\{\langle V^2(t)\rangle_{\xi} + \langle V^2(t)\rangle_{\xi'}\}^{-1/2}, \tag{A7}$$

where $\langle\ \rangle_\xi$ stands for the average expectation value with ξ fixed.

The averages in Eqs. (A7) and (A6) are carried out using the method of spectral distributions [35–37]. We obtain

$$\langle V_{kk'} V^\dagger_{kk'}\rangle = \tfrac{1}{4} U^2_{kk'} g_k g_{k'} \Delta_{kk'} \Delta\varepsilon_k \Delta\varepsilon_{k'} \times \left[\Delta^2_{kk'} + \tfrac{1}{6}\left(\Delta\varepsilon_k^2 + \Delta\varepsilon_{k'}^2\right)\right]^{-1/2}, \tag{A8}$$

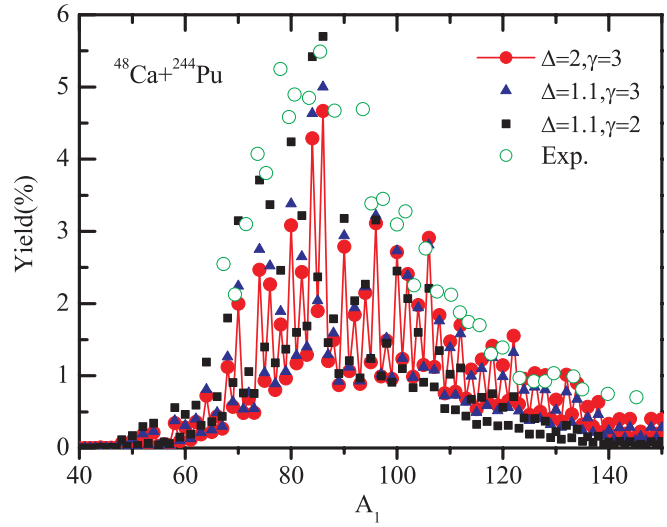

FIG. 15. (Color online) QF yield with different, but constant parameters of $\Delta_{k,k'}$ and $\gamma_{k,k'}$ for the reaction ^{48}Ca + ^{244}Pu.

$$\Delta\varepsilon_K = \sqrt{\frac{4\varepsilon_K^*}{g_K}}, \quad \varepsilon_K^* = \varepsilon^* \frac{A_K}{A}, \quad g_K = \frac{A_K}{12}. \tag{A9}$$

The local excitation energy is defined as $\varepsilon^* = E_x - U(A_1, A_2, R, \beta_1, \beta_2, J)$ [see Eq. (2.2)].

In principle, the parameters $\Delta_{k,k'}$ in Eq. (A4) and $\gamma_{k,k'}$ in Eq. (A5) are deformation dependent. Here, we have used the approximation that these parameters are constants, independent of deformations, which is very crude from the physical point of view. In Fig. 15, we demonstrate QF yields with different, but constant parameters. No essentially significant differences arise. However, it is clear that the deformation dependence of these parameters has to be considered in greater detail in our future work.

[1] S. Hofmann, Prog. Part. Nucl. Phys. **62**, 337 (2009).
[2] K. Morita *et al.*, J. Phys. Soc. Jpn. **73**, 2593 (2004).
[3] Y. Oganessian, Nucl. Part. Phys. **34**, R165 (2007).
[4] Y. Oganessian *et al.*, Phys. Rev. Lett. **104**, 142502 (2010).
[5] P. Armbruster, Annu. Rev. Nucl. Sci. **35**, 135 (1985).
[6] S. Hofmann, Rep. Prog. Phys. **61**, 639 (1998).
[7] S. Hofmann and G. Münzenberg, Rev. Mod. Phys. **72**, 733 (2000).
[8] S. Hofmann *et al.*, Eur. Phys. J. A **14**, 147 (2002).
[9] Y. T. Oganessian *et al.*, Phys. Rev. Lett. **83**, 3154 (1999); Nature **400**, 242 (1999); G. V. Danilyan *et al.*, Phys. At. Nucl. **63**, 1671 (2000); Y. T. Oganessian *et al.*, Phys. Rev. C **62**, 041604 (2000).
[10] G. G. Adamian *et al.*, Nucl. Phys. A **627**, 361 (1997); **633**, 409 (1998).
[11] A. Diaz-Torres, Phys. Rev. C **74**, 064601 (2006).
[12] G. G. Adamian *et al.*, Nucl. Phys. A **678**, 24 (2000).
[13] G. G. Adamian, N. V. Antonenko, S. P. Ivanova, and W. Scheid, Phys. Rev. C **62**, 064303 (2000).
[14] W. F. Li *et al.*, Europhys. Lett. **64**, 750 (2003).
[15] W. F. Li *et al.*, J. Phys. G **32**, 1143 (2006).
[16] Z. Q. Feng *et al.*, Nucl. Phys. A **816**, 33 (2009).
[17] G. Wolschin, Z. Phys. A **284**, 209 (1978).
[18] J. Q. Li and G. Wolschin, Phys. Rev. C **27**, 590 (1983).
[19] Z. Q. Feng *et al.*, Nucl. Phys. A **771**, 50 (2006).
[20] N. Wang, J. Q. Li, and E. G. Zhao, Phys. Rev. C **78**, 054607 (2008).
[21] M. H. Huang *et al.*, Chin. Phys. Lett. **25**, 1243 (2008).
[22] A. Diaz-Torres, G. G. Adamian, N. V. Antonenko, and W. Scheid, Phys. Rev. C **64**, 024604 (2001).
[23] G.G. Adamian, N.V. Antonenko, and W. Scheid, Phys. Rev. C **68**, 034601 (2003).
[24] Z. Q. Feng *et al.*, Nucl. Phys. A **836**, 82 (2010).
[25] M. Huang, Z. Gan, X. Zhou, J. Li, and W. Scheid, Phys. Rev. C **82**, 044614 (2010).
[26] P. Grangé, J.Q. Li, and H. A. Weidenmuller, Phys. Rev. C **27**, 2063 (1983).
[27] N. Wang, M. Liu, and X. Wu, Phys. Rev. C **81**, 044322 (2010).
[28] P. Möller *et al.*, At. Data Nucl. Data Tables **59**, 185 (1995).
[29] Z. Q. Feng *et al.*, High Energy Phys. Nucl. Phys. **31**, 366 (2007).
[30] J. Q. Li *et al.*, Phys. Lett. B **105**, 107 (1981).
[31] M. G. Itkis *et al.*, Nucl. Phys. A **734**, E13 (2004).
[32] M. G. Itkis *et al.*, Nucl. Phys. A **787**, 150c (2007).
[33] Y. T. Oganessian *et al.*, Phys. Rev. C **62**, 041604(R) (2000).
[34] Ch. E. Düllmann *et al.*, Phys. Rev. Lett. **104**, 252701 (2010).
[35] J. B. French *et al.*, Phys. Rev. C **3**, 94(R) (1971).
[36] F. S. Chang *et al.*, Ann. Phys. **66**, 137 (1971).
[37] S. Ayik *et al.*, Z. Phys. A **279**, 145 (1976).
[38] S. Ayik *et al.*, Z. Phys. A **277**, 299 (1976).